South African Journal of Chemical Engineering 27 (2019) 35–42

Contents lists available at ScienceDirect

South African Journal of Chemical Engineering

journal homepage: www.elsevier.com/locate/sajce

An attainable region approach for the recovery of iron and zinc from electric arc furnace dust

M.C. Siame[a], J. Kaoma[b], N. Hlabangana[c], G. Danha[d,*]

[a] Department of Civil and Chemical Engineering, College of Science, Engineering and Technology, University of South Africa, P/Bag X6, Florida, 1710, Johannesburg, South Africa
[b] Universal Mining and Chemical Industries Limited, Kafue Steel Plant, Plot 3944, Chibuku Road, Kafue, Lusaka, Zambia
[c] Department of Chemical Engineering, Faculty of Engineering and Technology, National University of Science and Technology, Private Bag A.C 939 Ascot, Bulawayo, Zimbabwe
[d] Department of Chemical, Materials and Metallurgical Engineering, Faculty of Engineering and Technology, Botswana International University of Science and Technology, Plot 10071 Boseja Ward, Private Bag 16 Palapye, Botswana

ARTICLE INFO

Keywords:
Electric arc furnace dust
Iron
Zinc
Optimization
Reclamation

ABSTRACT

This study investigated the application of the attainable region optimization technique to establish the optimum hybrid hydrometallurgical and pyro-metallurgical process conditions required to treat the electric arc furnace dust. The analysis of the results obtained showed that a combination of an agitation speed of 800 rpm, sodium hydroxide concentration of 8.0 mol/L and a leaching temperature of 80 °C were the optimum conditions for the hydrometallurgical process, while a roasting temperature of 1200 °C, carbon content of 35.27% and a roasting period of 36 h were the optimum conditions for the pyro-metallurgical process. The iron recovered from the dust was recycled in order to upgrade the iron content of the electric arc furnace charge, thereby reducing both process loses and process wastes.

1. Introduction

Universal Mining & Chemical Industries Ltd (UMCIL), Kafue steel plant was established in 1989 by Dr. Julius Kaoma, to invest in the exploitation of Zambian raw materials. The company sells 40% of its products within Zambian market and the rest is exported to neighboring countries such as Zimbabwe, South Africa, Botswana, Mozambique, Malawi, Democratic Republic of Congo, Rwanda, Burundi and Tanzania (Kaoma et al., 2013).

UMCIL is currently operating a 120 000 tons per year electric arc furnace (EAF) steel plant that turned into an integrated steel mill at the end of 2017 with the coming on stream of an iron ore mine and a direct reduction plant. The mini-steel plant encompasses a steel melting shop, rolling mill, 30 ton EAF, 30 ton ladle refining furnace and a 3 strand continuous casting machine of which the design capacity is 200 000 ton per year of 100 × 100/130 × 130 mm billets (Kaoma et al., 2013).

The company buys all sorts of scrap (Fig. 1) with grades like super heavy, heavy, medium heavy, light and very light in order to ensure that it does not run out of feed material. Specific types of scrap like rails, beams, old car bodies, cast iron, and alloyed steel are used with a stringent eye on undesirable components like non-ferrous material, explosive material e.g. guns and riffle shells, sealed pipes, gas cylinders and hydraulic cylinders. Explosive and sealed materials are removed and stored separately from a safety point of view.

UMCIL is currently experiencing a shortage of good quality scraps. Just like any other steel-making company in Zambia, UMCIL has never treated EAF dust before. The waste is safely disposed within the company premises at an established dump site awaiting the implementation of a technical approach to safely treat or recycle it.

Therefore, this study aims to establish hybrid hydrometallurgical and pyro-metallurgical process conditions required to treat the dust. The chemical composition of dust will provide options and conditions to decide about the best viable method for metal recovery.

An attainable region (AR) method will then be applied to establish optimum parameters such as agitation speed, lixiviant concentration, leaching temperature, carbon content, roasting time and roasting temperature for the maximum recovery of zinc and iron. The iron recovered from the electric arc furnace dust (EAFD) will then be recycled in order to upgrade the iron content of the EAF charge, thereby reducing both process loses and toxic wastes. Additional data, in the form of thermodynamic, mass, energy, entropy, heat integration, process design, reaction kinetics and economic considerations will then be detailed in

* Corresponding author.
E-mail address: danhag@biust.ac.bw (G. Danha).

https://doi.org/10.1016/j.sajce.2018.12.002
Received 7 September 2018; Received in revised form 1 November 2018; Accepted 7 December 2018

Fig. 1. Types of iron steel scraps used as feed material.

the next manuscript prior to the practical implementation of this project.

1.1. The attainable region method

The attainable region (AR) method is an analysis tool used to solve optimization problems (Hildebrandt et al., 1999). Analogous to the 'wanted region' in linear programming, the AR has guidelines for the construction of the achievable region and has some necessary conditions on how to obtain the optimum solution. The AR is defined as a set of all possible outcomes, for the system under consideration, that can be achieved using the fundamental processes operating within the system, and that satisfies all constraints placed on the system (Asiedu et al., 2014). The method uses a set of values of all the output variables that can be achieved by any possible process using a given feed. These output variables are then applied to the AR technique in order to define a possible geometric space within which the achievable points can be found (Hlabangana et al., 2016).

The main advantage of using the AR as an optimization tool lies in that it is model free and generic. The AR technique has been introduced to different fields of chemical engineering, namely: reactor synthesis (Ming et al., 2013), reaction engineering (Nisoli et al., 1997), biotechnology (Muvhiiwa et al., 2014), distillation (Kauchali et al., 2000), mineral processing (Khumalo et al., 2006), etc. In mineral processing, the technique has been extensively applied by several researchers in order to optimize factors such as comminution efficiency (Khumalo et al., 2008), residence time (Mulenga and Chimwani, 2013), ball size (Mulenga et al., 2011), particle breakage (Metzger et al., 2009), ball size distribution (Bwalya et al., 2014; Chimwani et al., 2015), slurry density (Danha et al., 2015) and slurry pool volume (Mulenga and Moys, 2014). However, the AR optimization method is yet to find applications in other mineral beneficiation operations such as flotation, leaching or smelting. The application of the attainable region optimization technique has also never been used before in the area of EAFD processing.

1.2. EAF dust

The production of steel using the EAF has become more prominent than any other process (Ruiz et al., 2007), because of its flexibility in operations, low capital investment and ability to use up to 100% scrap (iron containing) material as feed. Although the EAF method provides optimal and flexible ways of operations, material conservation in terms of waste reduction remains a challenge. On average 90% of the emissions rich in valuable metals are generated during technological operations and are not instantly recovered. In an EAF, the iron containing raw materials are melted at high temperatures of up to 1600 °C, and this enhances the elements to volatilize from the melted steel bath (Oustadakis et al., 2010). In a continuous melting process, the volatilized particles enter the gas phase before being cooled and oxidized to form fugitive matter known as the electric arc furnace dust (EAFD) (Guezennec et al., 2005).

On average, about 20 kg of steel dust is produced from every tonnage of recycled steel (Kukurugya et al., 2015). The EAFD is generated in different sizes and forms (Geldenhuis et al., 2002), depending on the type of the process used, the type of steel made and the quality of raw material used. The composition of EAFD is therefore directly linked to the chemistry of the metallic charge and refinery additives. The composition of the dust demands different forms of treatment (Havlik et al., 2005) and the possible methods of recycling valuable metals (e.g. iron) back to the steel-making process.

The presence of valuable metals in the EAFD and susceptibility of toxic heavy metals such as lead, chromium and cadmium has raised both environmental and economic concerns over ways and methods which can be employed to adequately handle the wastes (Chmielewski et al., 1997). Traditionally, treatment of the EAFD is done by stockpiling (Leclerc et al., 2003), but due to increased demand of steel and enormous increase in EAFD production, approximately two third of dust produced annually is currently processed for metal recovery (Pelino et al., 2002). Consequently, metal recovery has become more desirable because it provides an excellent feedstock (Grillo et al., 2014) and thereby reducing process and material loses.

The main purpose of treating EAFD is to remove zinc and other metal contaminants so that the iron containing material can be recovered and recycled to the steel-making process (Pelino et al., 2002). The EAFD is very rich in iron and many attempts to directly recycle it in steelmaking have proven rather difficult because of the complexity of its oxide combination. Direct recycle of EAFD to the electric arc furnace causes many operational problems such as the refractory failure and the complete filling of the gas off take (Buzin et al., 2017). Similarly, other unwanted elements at even low concentration reduce operation efficiency and life cycle of the furnaces which leads to production of poor quality steel. Adequate and proper minimization, characterization and utilization of dust including recovery require establishing both economic and environmental viable techniques of metal recovery (Wannakamb et al., 2013).

1.3. Treatment of electric arc furnace dust

The general techniques currently being used to process EAFD can be classified into pyro-metallurgical, hydrometallurgical and their combination (Havlik et al., 2006).

1.3.1. Hydrometallurgical methods

Generally, hydrometallurgical techniques target the processing of

Table 1
An overview of several hydrometallurgical techniques (Chmielewski et al., 1997).

Leaching Reagent	Process technique	Zinc recovery
NaOH	Selective leaching of zinc by dilute sodium hydroxide solution.	≥95%
$(NH4)_2CO_3$	Reduction roasting of Fe_3O_4 and leaching with Ammonium carbonate.	70–75%
H_2SO_4	Oxidative leaching with sulphuric acid at pH = 3 usually in autoclaves with counter-currently with precipitation of hematite.	Up to 75%
HCl	Pressure leaching with hydrochloric acid with hematite precipitation	98%

zinc, lead, non-ferrous metal oxides, etc. so as to increase the subsequent yield of iron oxides or sponge iron (Camci et al., 2002). The acidic and alkaline leaching techniques (Table 1) are the two most common hydrometallurgical methods used for treating the EAFD. Acidic leaching of the EAFD involves the dissolution of zinc into solution mainly using sulphuric acid which leaves a considerable amount of iron in the un-leached residue (Chmielewski et al., 1997). The main advantage of using sulphuric acid is its ability for better reaction kinetics with metal oxides in the dust and possible recycling of the solution in the second stage of the leaching process. The main disadvantage of using sulphuric acid in acidic leaching is its strength to dissolve both iron and zinc oxide creating a complication in treating the dissolved iron in the solution (Havlik et al., 2005).

Alkaline leaching of the EAFD is essentially the selective solubility of zinc and other metal oxides leaving the iron containing material in the residue. The major setback of alkaline leaching is the failure of the leach solution to dissolve complex and stable compounds of the dust (Havlik et al., 2006) such as the zinc ferrite ($ZnFe_2O_4$). However, other studies (Junca et al., 2015) suggest that more research needs to be done in order to improve this.

1.3.1.1. Leaching kinetics of EAFD. Leaching of EAFD is achieved by the dissolution of ZnO directly from the suspended zincate particles and from the complex zinc ferrite as shown in equations (1) and (2) (Jha et al., 2001).

$$ZnO(s) + 2NaOH\ (aq) \rightarrow Na_2ZnO_2(aq) + H_2O \quad (1)$$

$$ZnFe_2O_4\ (s) + 6NaOH\ (aq) \rightarrow Na_2ZnO_2\ (aq) + 2Na_2FeO\ (aq) + 3H_2O_{(L)} + 1.5O_{2(g)} \quad (2)$$

The component ZnO of the EAFD bulk solid phase reduces in size and is dissolved into the NaOH as suspensions of Na_2ZnO_2. The Na_2ZnO_2 suspensions then dissolve into the bulk liquid phase as shown in equation (3) (Youcai and Stanforth, 2000).

$$Na_2ZnO_2(s) + 2Na_3FeO_3(s) + 5H_2O(_L) \rightarrow Na_2Zn(OH)(aq) + 2Fe(OH)_3(s) + 6NaOH(aq) \quad (3)$$

The reduction of zinc from the EAFD and the increase of Na_2ZnO_2 in the aqueous solution follows the second order reaction rate;

$$\frac{dC_{zn^{2+}}}{dt} = k\left(C_{zn^{2+}n} - C_{zn^{2+}}\right)^2 \quad (4)$$

Where:

$C_{zn^{2+}}$ is the concetration of zinc going into solution at a particular time.
$C_{zn^{2+}n}$ is the concentration of zinc in saturated concetration of the leach solution.

The intergrated rate law for a second order leaching reaction for the boundary conditions at $t = 0$ to t and $C_{zn^{2+}} = 0$ to $C_{zn^{2+}}$ can be written as:

$$C_{zn^{2+}} = \frac{1}{C_{zn^{2+}}} + \frac{t}{C_{zn^{2+}n}} \quad (5)$$

Therefore the leaching rate equation for EAFD for varying leaching time can be obtained as shown in equation (6).

$$\frac{C_{zn^{2+}}}{t} = \frac{1}{\frac{1}{C_{zn^{2+}n}} + \frac{t}{C_{zn^{2+}}}} \quad (6)$$

At a fixed leaching time, the leaching rate follows a shrinking core model and therefore the values of k for each zinc fraction ratio during leaching process can be calculated using equation (7).

$$1 - \left(1 - C_{zn^{2+}}\right)^{\frac{1}{3}} = \oint_0^t C_{zn^{2+}} dt = k't \quad (7)$$

The leaching rate constant k can be expressed as in equation (8) (Levenspiel, 1999):

$$k = k_n exp\left(\frac{-ER}{T}\right) \quad (8)$$

Where:

k_n is the temperature dependent factor.
E the apparent activation energy
R is the universal gas constant 8.314 J.mol^{-1}. K^{-1}

From equation (8), if natural logarithms are taken on both sides:

$$\ln k = ln\ k_n + \left(\frac{-E}{R}\right)\frac{1}{T} \quad (9)$$

A plot of the leaching rate and reciprocal of the absolute temperature in equation (9) indicates a linear first order relationship (Levenspiel, 1999). In such a plot, $\ln k_n$ would be the intercept and $\frac{-E}{R}$ the slope.

1.3.2. Pyro-metallurgical methods

Essentially, pyro-metallurgical treatment of electric arc furnace dust is done using two types of techniques, namely, the metal recovery and smelting process (Kim et al., 2006). In the metal recovery process, iron oxide (Fe_2O_3) is not melted but reduced to FeO while in the smelting process the iron oxide is melted and reduced to iron. In these two processes, zinc is obtained as a vapour and separated from the reduction of zinc oxide. In metal recovery process, combustion of solid fuels enhances the energy controlled reduction process whose exhaust gas also reduces the zinc oxide (Siwka et al., 2012). Oxides of iron are converted into highly reduced iron containing metals such as pellets by an effective degree of metallization. The disadvantages of pyro-metallurgical techniques are that they require a high consumption of electricity and also result in the creation of raw zinc oxide with low commercial value (Kia, 1997).

1.3.2.1. Kinetics of reduction of oxides of iron from EAFD. The kinetic reactions of carbothermic reduction of oxides of iron from the EAFD depends mainly on the rate at which the iron oxide is converted to metallic iron. The reaction involves various reduction steps which are controlled by diffusion and phase-chemical boundaries (Hahn and Chang, 1998). The diffusion controlled reaction involves the penetration of the reducing gas into the iron oxide particle layer and the release of product gas outward through the iron layer. The diffusion rate expression is described by equation (9) and if the reaction is chemically controlled (Kukurugya et al., 2015) then equation (10) is applicable. Equation (10) represents the amount of iron in solution during the reaction while equation (11) evaluates the amount of iron actually reduced during the reaction(Levenspiel, 1999).

$$1 - \frac{2}{3}Fe^{2+}(1 - Fe^{2+})^{\frac{2}{3}} = kt \quad (10)$$

$$1 - (1 - \%Fe^{2+})^{\frac{1}{3}} = \oint_0^t \%Fe^{2+} dt = k_T t \quad (11)$$

Where: %Fe is the percentage by mass of iron reduced during the reaction and k_T the temperature dependante reaction coefficient.

The chemical boundary controlled reaction involves the diffusion of the reducing gas (in our case carbon monoxide) into the boundary across the outer layer of the iron oxide particle (Kim et al., 2006). If the plot of percentage of iron oxide reduced to metallic iron $(1 - \%Fe^{2+})^{\frac{1}{3}}$ and roasting time t, is linear, then the rate of reaction is chemical reaction controlled and the values of the rate constant k can be obtained

from equation (12).

$$k = k_n exp\left(\frac{-ER}{T}\right) \quad (12)$$

Where:

k_n is the temperature dependent coefficient factor,
E the activation energy
R is the gas constant.

2. Materials and methods

2.1. Particle size analysis

A prepared sample of the EAFD was dried for 30 min in an oven set at a temperature of 50 °C (Hlabangana et al., 2018). Cone and quartering was then performed on the dried sample in order to split it into smaller 100 g samples for sieve analysis. The homogenized 100 g sample was then added to the stack of eight clean sieves, 200 mm in diameter, arranged in descending order of mesh sizes from 350 μm, 240 μm, 150 μm, 100 μm, 72 μm, 52 μm, 36 μm and the pan below (Hlabangana et al., 2017). The stack was then mounted on an electrically powered mechanical sieve shaker, and wet sieved for 20 min. The wet sieve analysis used is as a good and precise a method of particle size analysis as compared to any laser diffraction techniques. Danha et al. (2015) did use the Malvern Particle Size Analyser model 2000MU on a different ore and found that using the wet cell produced better results when compared to the dry cell, mainly due to the dispersion ability of water and not necessarily because of the effect of the ultrasound mechanism.

2.2. Determination of chemical and elemental composition

After sieve analysis, a homogenized 20.0 g of the EAFD was sampled and used for XRD analysis. We also transferred another homogenized 10.0 g sample of the EAFD into a 500 ml conical flask. The sample was transferred into a conical flask and then prepared for acidic digestion by first hydrolysing it with 20 ml of water and then assimilated by adding 60 ml of aqua-rigger solution in the ratio of 1:2 (Danha et al., 2017). The mixture was then transferred to a hot plate and heated for 30 min at a set temperature of 90 °C. During the 30 min of sample digestion, the atomic absorption spectrometer (AAS, Varian AA220) was calibrated using standard solutions. This in-situ procedure was done in order to maximize the degree of certainty of the results as well as minimize the risk of contamination from previously analyses. The digested sample was then taken to the spectra for elemental analysis.

2.3. Leaching of the EAFD

Leaching of the homogenized EAFD was carried out in three stages. The aim of the first stage of leaching was to determine the optimum agitation speed required for effective leaching. The first leaching stage was performed by adding 10 g of the EAFD sample into a 1000 ml glass vessel equipped with a stirring agitator, and placed in a temperature controlled water bath set at 65 °C. About 100 ml of 2 mol/L solution of sodium hydroxide was then added to the sample in the vessel and the slurry agitated at 500 rpm for 110 min. More experimental runs were performed at different agitation speeds ranging from 500 rpm to 900 rpm, in order to investigate the effect of agitation speed on leaching. The slurry from each set of leaching was filtered and the filtrate analysed for zinc leaching efficiency (amount of zinc in the filtrate) by the AAS 220 spectrometer.

After the first leaching stage, the optimum agitation efficiency obtained was then used in the second leaching stage. The aim of the second leaching stage was to establish the optimum concentration of sodium hydroxide required to effectively leach the dust. About 100 ml of sodium hydroxide solution of concentrations ranging between 2 mol/L and 10 mol/L were used in a series of leaching tests on a 10 g EAFD sample. The agitation speed, leaching time and solution temperature were all kept constant at 800 rpm, 110 min and 65 °C, respectively. The slurry from each set of tests in this investigation was also filtered and the filtrate analysed for zinc leaching efficiency.

The aim of the third leaching stage was to investigate the optimum leaching temperature of sodium hydroxide required to effectively leach the dust. For this leaching stage, 100 ml of sodium hydroxide at a concentration of 6 mol/L was used for a series of leaching tests at a constant agitation speed of 800 rpm and a fixed leaching time of 110 min, while changing the solution temperature from 25 °C to 100 °C. The Liquid (L): Solid (S) ratio was kept constant at 10 ml/g for all the leaching tests conducted in this experimental work. This was in accordance to the AR optimization technique applied that requires some parameters to be fixed while those that needed to be optimized are varied.

2.4. Filtration of the EAFD leach slurry

After establishing the optimum agitation speed, concentration of sodium hydroxide and leaching temperature, the combination of these optimized parameters were used in carrying out 8 batch leaching tests, on 10 g samples of the EAFD and at a fixed leaching period of 110 min. The slurry from the leaching tests was transferred to the filter funnel of an electric powered pressure filter which was covered by a filter cloth. Filtration was then carried out until the breaking point of the filter cake. The cake was dried in an oven at 50 °C for 30 min and then crushed into powder which was taken for carbothermic roasting.

2.5. Roasting of the EAFD leach residue

Carbothermic treatment of the EAFD leach residue entailed preparation of carbon containing material (coal), followed by determination of the moisture, volatile matter and fixed carbon content of the coal. This was followed by blending the fine (- 75 μm + 25 μm) milled coal with EAFD and heating the mixture at elevated temperatures of up to 1400 °C.

In order to achieve this, a 10 g sample of leach residue from the filtration process was blended with 20 g of a low rank coal and the mixture was put into a silica carbide crucible. The crucible was then placed in an electric powered laboratory scale furnace. The sample was heated for 6, 12, 36 and 48 h at a temperature of 800 °C. The procedure was repeated for temperatures of 1000, 1200 and 1400 °C respectively. The samples were analysed using the AAS 220 spectra after each heating interval (Danha et al., 2017).

An extended method of the Attainable Region involving Gibbs Free Energy-Enthalpy plots will be a good way of showing the limits of performance for this process. However, from the compounds in Equations (1) and (2), lack of thermodynamic data for the complex compounds of zinc ferrite and sodium zincate make it difficult to analyse and predict the results of leaching EAFD using this NaOH solution. This is usually a complex problem in many of the mineral processing industries but in this case it can be assumed that only ZnO is our complex EAFD sample. If another method is taken of reducing zinc oxide with carbon or carbon monoxide via the pyrometallurgy process, the following equations are involved:

$$2ZnO + C \rightarrow 2Zn + CO_2 \quad (13)$$

$$ZnO + CO \rightarrow Zn + CO_2 \quad (14)$$

and overall material balance given as:

$$3ZnO + C + CO \rightarrow 3Zn + 2CO_2 \quad (15)$$

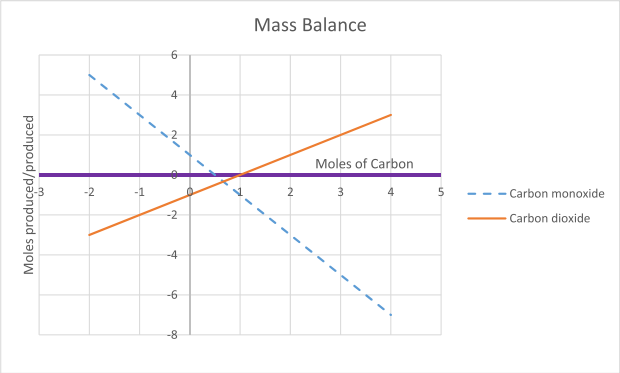

Fig. 2. Mass balance for producing Zn from one mole of ZnO (-ve means product and +ve means reactant).

3. Results and discussion

Fig. 2 shows that carbon monoxide and carbon can be added to zinc oxide to produce zinc with carbon dioxide being the by-product. If it is assumed that the EAFD is composed of ZnO, G-H plots can be used to show the thermodynamic analysis of producing zinc from one mole of ZnO. This is shown in Figs. 3 and 4 for temperatures of 25 °C and 1000 °C. Fig. 3 shows that it is not possible to add carbon to one mole of zinc oxide and produce zinc at 25 °C because the Gibbs Free energy is positive. But from a mass balance perspective, the process is feasible at 25 °C if carbon monoxide is added and this is also dependent on kinetics. However, at 1000 °C as shown in Fig. 4, addition of carbon to make zinc is feasible at the expense of producing carbon monoxide or carbon dioxide and the process is endothermic. Figs. 2–4 shows two options for getting zinc from zinc oxide. The first one has limits on which one can add carbon monoxide and produce zinc with carbon and carbon dioxide as by-products at 25 °C. This suggests an ideal application for pyrometallurgical processes especially when considering low temperatures. The second one is to add carbon and carbon dioxide to produce zinc with carbon monoxide as a by-product at 1000 °C. Remember that this analysis has been made on ZnO using C and CO because we have thermodynamic data of it for G and H. The same analysis can be done using NaOH only when we have the Gibbs Free energy for $ZnFe_2O_4$ and Na_2ZnO_2(aq).

Fig. 5 shows a particle size distribution (PSD) plot of an EAFD sample used as feed material in this study. It can be seen from this plot that the mass of particles retained on each sieve size expressed as a percentage of the total mass (100 g) of the sieved sample is plotted against the sieve size. The Figure reveals that about half of the mass of the dust was retained on the 150 µm sieve which indicates the degree of fineness of the EAFD. Size of the EAFD particles affects surface of the

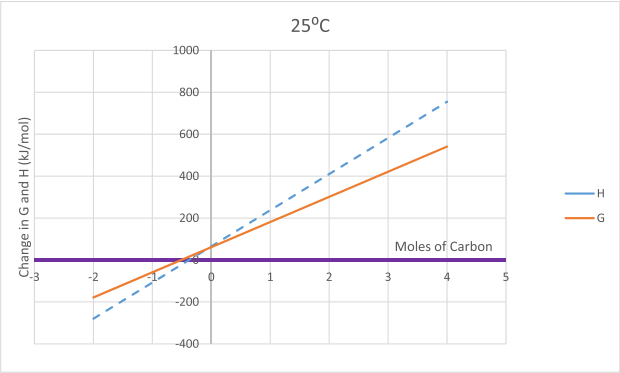

Fig. 3. Changes in Gibbs Free energy and Enthalpy for producing Zn from ZnO using C and CO at 25 °C.

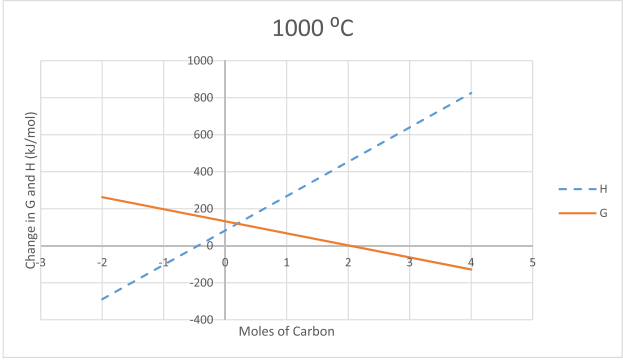

Fig. 4. Changes in Gibbs Free energy and Enthalpy for producing Zn from ZnO using C and CO at 1000 °C.

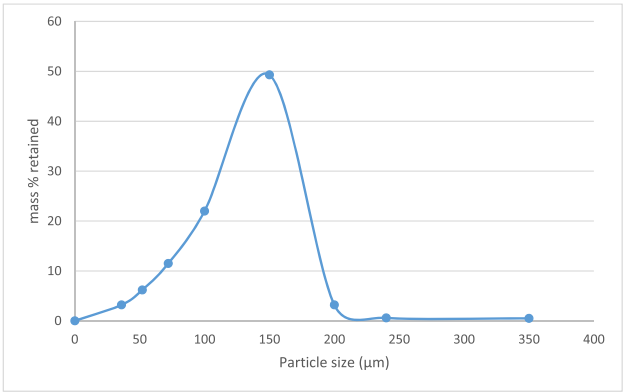

Fig. 5. Percentage of mass retained vs. particle size.

particles per unit volume and therefore the rate at which individual particles can participate in a chemical reaction (Ujam and Enebe, 2013). For example, during a liquid-solid phase contact reaction, the resistance to flow is dominated and influenced by the size and shape of the particles. Larger and spherical particles flow easily than the high aspect ratio particles because the bigger the particle the higher is the suspension viscosity. The PSD of many steel dusts range from sub-micron to more than 500 µm in size (Guezennec et al., 2005).

Fig. 6 shows an attainable region (AR) plot of the main chemical composition of the EAFD and the relative abundance of these chemical components in the dust. The data points are discrete, hence their connection using a dotted and not a continuous line. The composition of EAFD is directly linked to the chemistry of the metallic charge and refinery additives. The dotted line that joins the data points is not a model fit to experimental data, but was added in order to make the trend easy to follow. The AR plot shows that the oxides of iron

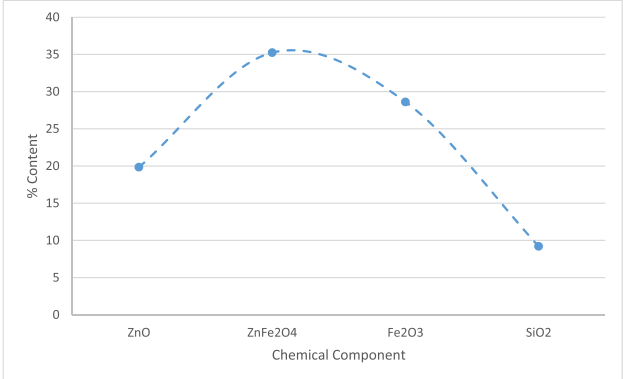

Fig. 6. Percentage content vs. chemical component.

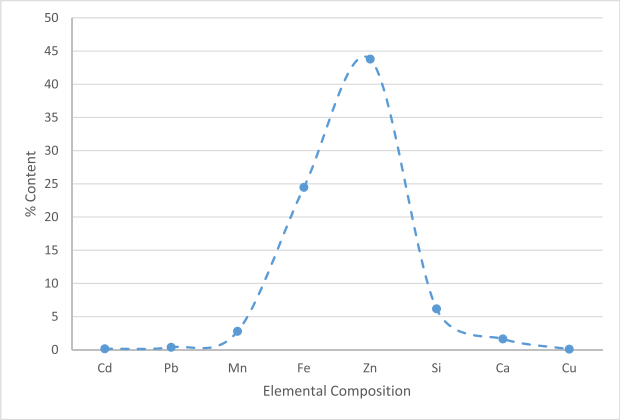

Fig. 7. Percentage content vs. elemental composition.

(28.62%), zinc (19.85%) and their combination (35.25%) when added together give a total of 83.72% of the chemical composition of the dust. This chemical analysis provided the statistics that justified the treatment of EAFD for the recovery of both zinc and iron. The presence of zinc in oxide form demands use of a hydrometallurgical method in order to recover the metal, while the presence of iron in oxide form demands the use of a pyro-metallurgical technique to reclaim the metal. Since both oxides are present in sizable quantities in the EAFD, the two treatment methods were applied consecutively in order to process the dust for both zinc and iron metal recovery.

Fig. 7 shows an AR plot of the main elemental composition and their relative abundance in the EAFD. The dotted line was again added in order to understand the process trend. The high percentage of elemental zinc (24.46%) and iron (43.79%) contents in the dust was a conclusive evidence of the need to carry out this study of recovering these metals using either hydrometallurgical, pyro-metallurgical or a combination of the two techniques. A hydrometallurgical approach (leaching with NaOH) was the technique employed to treat the EAFD for selective zinc recovery, while a pyrometallurgical method (carbothermic roasting) was used next in reclaiming iron from its oxides in the leached dust.

Fig. 8 depicts an AR plot of the effect of agitation speed on the leaching efficiency of zinc. A constant solution temperature of 65 °C, residence time of 110 min, NaOH concentration of 2.0 mol/L with varying speeds of agitation were used as the experimental conditions. The results show that as the speed of agitation increases, the efficiency of zinc extraction increases up to a limit value and then start decreasing. The increase in stirring speed reduced the thickness of the slurry layer and therefore increased the eddy diffusion of the material which subsequently transferred the particles to the bulk of the solution.

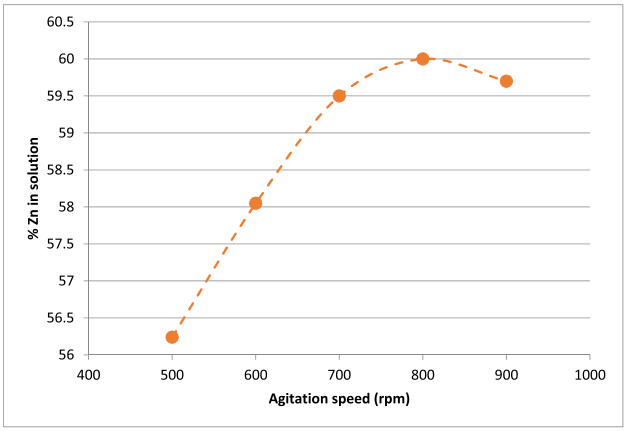

Fig. 8. Concentration of zinc in solution vs. Agitation speed.

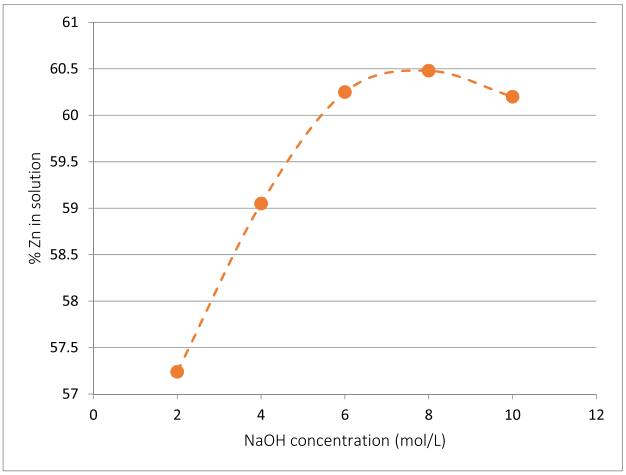

Fig. 9. Concentration of zinc in solution vs. NaOH concentration.

The AR plot shows that the optimum agitation speed for maximum zinc recovery was 800 rpm, under the experimental conditions tested. As the speed of agitation was increased beyond 800 rpm, the contents of the vessel started to centrifuge, thereby reducing the intimate contact between the lixiviant and the filtrate. This reaction condition negatively affected the extraction efficiency of zinc.

Fig. 9 shows an AR plot for the results of leaching the dust using an agitation speed of 800 rpm, solution temperature of 65 °C and a residence time of 110 min with different concentrations of sodium hydroxide. The area bounded by the curve and the x-axis represents the different combinations of the concentration of zinc in solution obtained from leaching with a certain concentration of NaOH solution. The leaching efficiency of zinc increases with increase in concentration of alkaline solution used, up to a limit. A further increase in solution concentration increases the viscosity of the leaching solution thereby reducing the solid-liquid separation efficiency. The AR plot shows that for the objective function of maximizing the concentration of zinc in solution, the optimum concentration of NaOH to be used in order to achieve this is the one that corresponds to the turning point on the curve. According to the AR optimization technique, an optimum condition for achieving a desired objective is often found on the boundary of the curve, and always located at the turning point. Therefore, a NaOH concentration of 8.0 mol/L was required in order to obtain a maximum concentration of zinc in solution of 60.5%.

Fig. 10 shows an AR plot obtained from leaching the EAFD using an agitation speed of 800 rpm, NaOH concentration of 8.0 mol/L, a residence time of 110 min while varying the leaching temperature. According to the guiding principles of the AR optimization technique, the

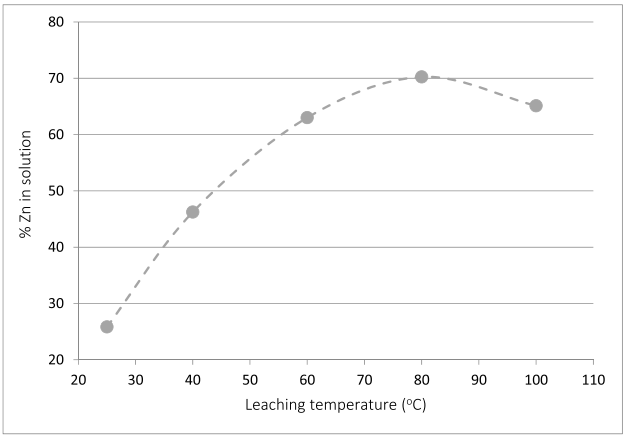

Fig. 10. Concentration of zinc in solution vs. leaching temperature.

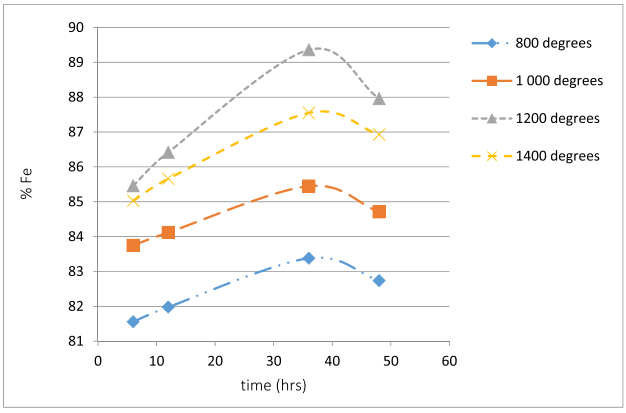

Fig. 11. Concentration of iron in the leach residue vs. roasting time.

area bounded by the curve and the x-axis represents all the possible coordinates of leaching temperature and concentration of zinc in solution, under the experimental conditions investigated. The optimum coordinates for achieving a desired objective function are found on the peripherals or boundaries of the attainable region. For the desired objective of maximizing the concentration of zinc in solution, the AR technique reveals that an optimum temperature of 80 °C results in a maximum zinc concentration of 70% in solution.

Fig. 11 shows attainable region plots of the concentration of iron in the leached residue against roasting time for a fixed carbon content of 25.04% and under different roasting temperatures. It can be observed from Fig. 11 that the amount of iron recovered increases with an increase in the roasting time and roasting temperature, up to a limit. Beyond the turning point (1200 °C), the product (iron) and the by-products (carbon monoxide) begin to react, thereby shifting the position of equilibrium towards the reactants. This phenomenon is observed in all the plots presented in Fig. 11. The AR plots indicate that in order to archive the objective function of maximizing the amount of iron in the roasted residue, a roasting time of 36 h and a roasting temperature of 1200 °C were the optimum parameters to employ, under the experimental conditions tested.

Fig. 12 shows attainable region plots of the concentration of iron in the roasted leach residue against the concentration of carbon in the coal that was used as the reducing agent. The investigation was carried out for roasting periods ranging between 6 and 48 h, and at a constant roasting temperature of 1200 °C. The Figure reveals that in order to obtain a maximum iron content of 89.87%, the optimum parameters required to achieve this was a carbon content of 35.27% and a roasting time of 36 h.

Fig. 13 is a plot of equation (9), in which the leaching rate is plotted

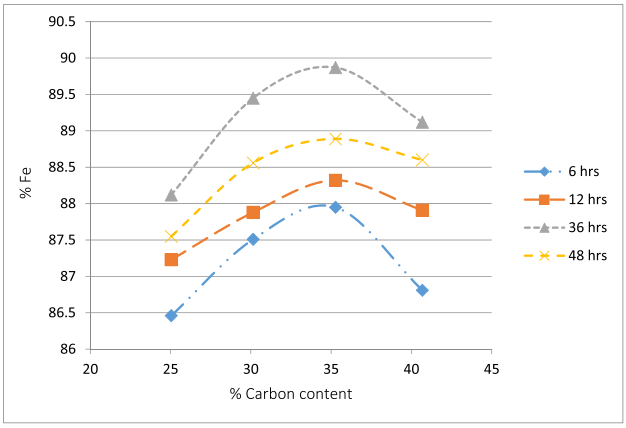

Fig. 12. Concentration of iron in the leach residue vs. coal carbon content.

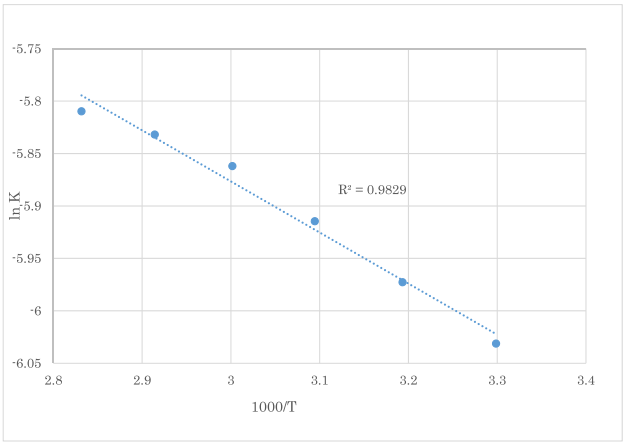

Fig. 13. Arrhenius plot of the leaching kinetics.

against the reciprocal of absolute temperature. The linear plot of Fig. 13 implies that the leaching kinetics of the EAFD follow a linear first order relationship and the apparent activation energy was calculated to be 7.069 kJ/mol, This plot also indicates that the leaching of zinc from EAFD was an endothermic reaction and the chemical reaction controlled the rate between 30 and 80 °C.

Fig. 14 is a plot of equation (10) and shows the relationship between $(1-\%Fe^{2+})^{\frac{1}{3}}$ and roasting time for a temperature range from 1073.15 K to 1673015 K. From Fig. 14, it can be observed that this relationship is linear and therefore k_T can be expressed as in equation (11) from where the values of k_T at particular reduction temperature can be evaluated. The activation energy of the carbothermic reaction is calculated from the plot of $\ln k_T$ and the reciprocal of absolute temperature as shown in Fig. 13. The activation energy was calculated to be −5.06 kJ/mol which implies that the reaction was exothermic and chemical reaction controlled.

4. Conclusions

PSD analysis of the EAFD showed that almost 50% of the material was retained on the 150 µm sieve size. This type of size distribution affected the surface per unit volume of the particles and therefore determined the rate at which individual particles participated in the pyrometallurgical and hydrometallurgical reactions. Application of the attainable region optimization technique on the experimental data, established the hydrometallurgical and pyrometallurgical conditions for the optimum leaching of zinc and maximum recovery of iron from the EAFD. A combination of an agitation speed of 800 rpm, sodium hydroxide concentration of 8.0 mol/L and a leaching temperature of 80 °C were the optimum conditions for the hydrometallurgical process.

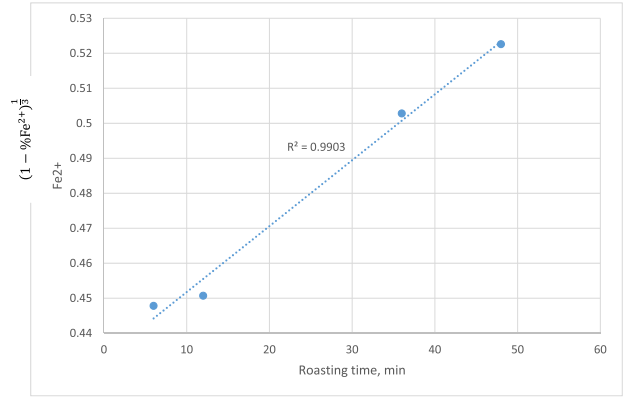

Fig. 14. Plot to show the reduction of oxides of iron.

For the pyrometallurgical process, the optimum conditions were a roasting temperature of 1200 °C, carbon content of 35.27% and a roasting period of 36 h.

Conflicts of interest

This manuscript has not been published previously and is not under consideration for publication elsewhere.

References

Asiedu, N.Y., Hildebrandt, D., Glasser, D., 2014. Batch distillation targets for minimum energy consumption. Ind. Eng. Chem. Res. 53, 2751–2757.

Buzin, P.J.W.K., Heck, N.C., Vilela, A.C.F., 2017. EAF Dust: an Overview on the Influences of Physical, Chemical and Mineral Features in its Recycling and Waste Incorporation Routes.

Bwalya, M.M., Moys, M.H., Finnie, G.J., Mulenga, F.K., 2014. Exploring ball size distribution in coal grinding mills. Powder Technol. 257, 68–73.

Camci, L., Aydin, S., Arslan, C., 2002. Reduction of iron oxides in solid wastes generated by steelworks. Turk. J. Eng. Environ. Sci. 26, 37–44.

Chimwani, N., Mulenga, F.K., Hildebrandt, D., 2015. Ball size distribution for the maximum production of a narrowly-sized mill product. Powder Technol. 284, 12–18.

Chmielewski, A.G., Urbanski, T.S., Migdal, W., 1997. Separation technologies for metals recovery from industrial wastes. Hydrometallurgy 45, 333–344.

Danha, G., Hildebrandt, D., Glasser, D., Bhondayi, C., 2015. A laboratory scale application the attainable region technique on a platinum ore. Powder Technol. 27, 414–419.

Danha, G., Bhondayi, C., Hlabangana, N., Hildebrandt, D., 2017. Determining the PGM bearing mineral phase in the UG2 ore. Powder Technol. 315, 236–242.

Geldenhuis, J.M.A., 2002. Recovery of valuables from flue dust fines. Miner. Eng. 15, 95–98.

Grillo, F.F., Coleti, J.L., Espinosa, D.C.R., Oliveira, J.R., Tenorio, J.A.S., 2014. Zn and Fe recovery from electric arc furnace dusts. Mater. Trans. 55, 351–356.

Guezennec, A.G., Huber, J.C., Patisson, F., Sessiecq, P., Barat, J.P., Ablitzer, D., 2005. Dust formation in electric arc furnace: birth of the particles. Powder Technol. 157, 2–11.

Hahn, Y.B., Chang, K.S., 1998. Mathematical modeling of the reduction process of iron ore particles in two stages of twin-fluidized beds connected in series. Metall. Mater. Trans. 29, 969–977.

Havlik, T., Turzakova, M., Stopic, S., Friedrich, B., 2005. Atmospheric leaching of EAF dust with diluted sulphuric acid. Hydrometallurgy 77, 41–50.

Havlik, T., Souza, B.V., Bernardes, A.M., Schneider, I.A.H., Miskufova, A., 2006. Hydrometallurgical processing of carbon steel EAF dust. J. Hazard Mater. B 135, 311–318.

Hildebrandt, D., McGregor, C., Glasser, D., 1999. The attainable region and pontryagin's maximum principle. Ind. Eng. Chem. Res. 38, 652–659.

Hlabangana, N., Danha, G., Hildebrandt, D., Glasser, D., 2016. Use of the attainable region approach to determine major trends and optimize particle breakage in a laboratory mill. Powder Technol. 291, 415–419.

Hlabangana, N., Danha, G., Bwalya, M.M., Hildebrandt, D., Glasser, D., 2017. Application of the attainable region method to determine optimal conditions for milling and leaching. Powder Technol. 317, 400–407.

Hlabangana, N., Danha, G., Muzenda, E., 2018. Effect of ball and feed particle size distribution on the milling efficiency of a ball mill: an attainable region approach. S. Afr. J. Chem. Eng. 25, 79–84.

Jha, M.K., Kumar, V., Singh, R.J., 2001. Review of hydrometallurgical recovery of zinc from industrial wastes. Resour. Conserv. Recycl. 33, 1–22.

Junca, E., Restivo, T.A.G., Espinosa, D.C.R., Tenório, J.A.S., 2015. Application of stepwise isothermal analysis method in the kinetic study of reduction of basic oxygen furnace dust. J. Therm. Anal. Calorim. 120, 1913–1919.

Kaoma, J., Lungu, C.V., Chilumbu, D., Musonda, L., Maseka, C., Mulenga, P., 2013. Universal Mining and Chemical Industries Limited (UMCIL) Environmental Impact Assessment (EIA) Report Submitted to Environment Council of Zambia. pp. 1–103.

Kauchali, S., McGregor, C., Hildebrandt, D., 2000. Binary distillation re-visited using the attainable region theory. Comput. Chem. Eng. 24, 231–237.

Khumalo, N., Glasser, D., Hildebrandt, D., Hausberger, B., Kauchali, S., 2006. The application of the attainable region analysis to comminution. Chem. Eng. Sci. 61, 5969–5980.

Khumalo, N., Glasser, D., Hildebrandt, D., Hausberger, B., 2008. Improving comminution efficiency using classification: an attainable region approach. Powder Technol. 187, 252–259.

Kia, D.K., 1997. Recovery of Zinc from Zinc Ferrite and Electric Arc Furnace Dust (A Thesis submitted to the Department of Materials & Metallurgical Engineering at Queen's University, Canada). .

Kim, B.S., Yoo, J.M., Park, J.T., 2006. A kinetic study of the carbothermic reduction of zinc oxide with various additives Meter. Sci. Trans. 47, 2421.

Kukurugya, F., Vindt, T., Havlík, T., 2015. Behavior of zinc, iron and calcium from electric arc furnace (EAF) dust in hydrometallurgical processing in sulfuric acid solutions: thermodynamic and kinetic aspects. Hydrometallurgy 154, 20–32.

Leclerc, N., Meux, E., Lecuire, J.M., 2003. Hydrometallurgical extraction of zinc from zinc ferrites. Hydrometallurgy 70, 175–183.

Levenspiel, O., 1999. Chemical Reaction Engineering, third ed. John Wiley and Sons, pp. 27–356.

Metzger, M.J., Glasser, D., Hausberger, B., Hildebrandt, D., Glasser, B.J., 2009. Use of the attainable region analysis to optimize particle breakage in a ball mill. Chem. Eng. Sci. 64, 3766–3777.

Ming, D., Glasser, D., Hildebrandt, D., 2013. Application of the attainable region theory to batch reactors. Chem. Eng. Sci. 99, 203–214.

Mulenga, F.K., Chimwani, N., 2013. Introduction to the use of the attainable region method in determining the optimal residence time of a ball mill. Int. J. Miner. Process. 125, 39–50.

Mulenga, F.K., Moys, M.H., 2014. Effects of slurry pool volume on milling efficiency. Powder Technol. 256, 428–435.

Mulenga, F.K., Moys, M.H., Glasser, D., Hildebrandt, D., 2011. An attainable region analysis of the effect of ball size on milling. Powder Technol. 210, 36–46.

Muvhiiwa, R.F., Hildebrandt, D., Glasser, D., Matambo, T., 2014. Applying the attainable region approach to biogas production. In: AIChE Conference Proceedings, vol. 11. pp. 16–21.

Nisoli, A., Malone, M.F., Doherty, M.F., 1997. Attainable regions for reaction with separation. AIChE J. 43, 374–387.

Oustadakis, P., Tsakiridis, P.E., Katsiapi, A., Agatzini-Leonardou, S., 2010. Hydrometallurgical process for zinc recovery from electric arc furnace dust (EAFD), Part I: characterization and leaching by diluted sulphuric acid. J. Hazard Mater. 179, 1–7.

Pelino, M., Karamanov, A., Pisciella, P., Crisucci, S., Zonetti, D., 2002. Vitrification of electric arc furnace dusts. Waste Manag. 22, 945–949.

Ruiz, O., Clemente, C., Alonso, M., Alguacil, F.J., 2007. Recycling of an electric arc furnace flue dust to obtain high grade ZnO. J. Hazard Mater. 141, 33–36.

Siwka, J., Sorek, A., Nieler, M., 2012. Dust arising during steelmaking process. Journal of achievements in materials and manufacturing engineering 55, 772–776.

Ujam, A., Enebe, K., 2013. Experimental analysis of particle size distribution using electromagnetic sieve. American Journal of engineering research 2, 77–85.

Wannakamb, S., Manuskijsamrun, S., Buggakupta, W., 2013. The use of electric arc furnace dust from steel recycling in ceramic glaze. Suranaree J. Sci. Technol. 20, 329–337.

Youcai, Z., Stanforth, R., 2000. Integrated hydrometallurgy process for production of Zinc from electric arc furnace dust in alkaline solution. Journal of hazardous material 80, 223–240.